LETTER

Aggregate dust particles at comet 67P/Churyumov–Gerasimenko

Mark S. Bentley[1]*, Roland Schmied[1]*, Thurid Mannel[1,2]*, Klaus Torkar[1], Harald Jeszenszky[1], Jens Romstedt[3], Anny-Chantal Levasseur-Regourd[4], Iris Weber[5], Elmar K. Jessberger[5], Pascale Ehrenfreund[6,7], Christian Koeberl[8,9] & Ove Havnes[10]

Comets are thought to preserve almost pristine dust particles, thus providing a unique sample of the properties of the early solar nebula. The microscopic properties of this dust played a key part in particle aggregation during the formation of the Solar System[1,2]. Cometary dust was previously considered to comprise irregular, fluffy agglomerates on the basis of interpretations of remote observations in the visible and infrared[3–6] and the study of chondritic porous interplanetary dust particles[7] that were thought, but not proved, to originate in comets. Although the dust returned by an earlier mission[8] has provided detailed mineralogy of particles from comet 81P/Wild, the fine-grained aggregate component was strongly modified during collection[9]. Here we report *in situ* measurements of dust particles at comet 67P/Churyumov–Gerasimenko. The particles are aggregates of smaller, elongated grains, with structures at distinct sizes indicating hierarchical aggregation. Topographic images of selected dust particles with sizes of one micrometre to a few tens of micrometres show a variety of morphologies, including compact single grains and large porous aggregate particles, similar to chondritic porous interplanetary dust particles. The measured grain elongations are similar to the value inferred for interstellar dust and support the idea that such grains could represent a fraction of the building blocks of comets. In the subsequent growth phase, hierarchical agglomeration could be a dominant process[10] and would produce aggregates that stick more easily at higher masses and velocities than homogeneous dust particles[11]. The presence of hierarchical dust aggregates in the near-surface of the nucleus of comet 67P also provides a mechanism for lowering the tensile strength of the dust layer and aiding dust release[12].

MIDAS, the Micro-Imaging Dust Analysis System[13,14], is the first space-borne atomic force microscope (AFM) and a unique instrument designed to measure the size, shape, texture and microstructure of cometary dust. Flying on the Rosetta spacecraft, it collects dust on sticky targets during passive exposures and images its three-dimensional topography with an unprecedented nanometre to micrometre resolution[13].

Cometary dust was first collected in mid-November 2014. Here, we focus on particles collected from then until the end of February 2015. The collected particles cover a range of sizes from tens of micrometres down to a few hundred nanometres, and have various morphologies, from single grains to aggregate particles with different packing densities. Five examples are presented here.

Figure 1 shows topographic images (height fields) of three particles (A, B and C). We refer to particles A and C as compact, because their sub-units (hereafter grains) are tightly packed; particle B appears to be a homogeneous grain. The next example (D) is also a compact particle, scanned with a higher lateral resolution of 80 nm (Fig. 2)—a factor four better than the previous scan. The final particle (E), presented in Fig. 3,

is best described as a loosely packed, 'fluffy' aggregate comprising many grains. Detailed collection times and geometries for all particles can be found in Extended Data Figs 1–3.

Aided by the three-dimensional nature of the data, individual grains can be identified, as shown in Figs 1b, 2b and 3b. The properties of these particles and their grains are summarized in Table 1 for particles A–D and in Fig. 3d for particle E. Because particle E extends beyond the edge of the scanned area, only lower limits for its dimensions can be given. All further calculations and discussion refer to only this visible region.
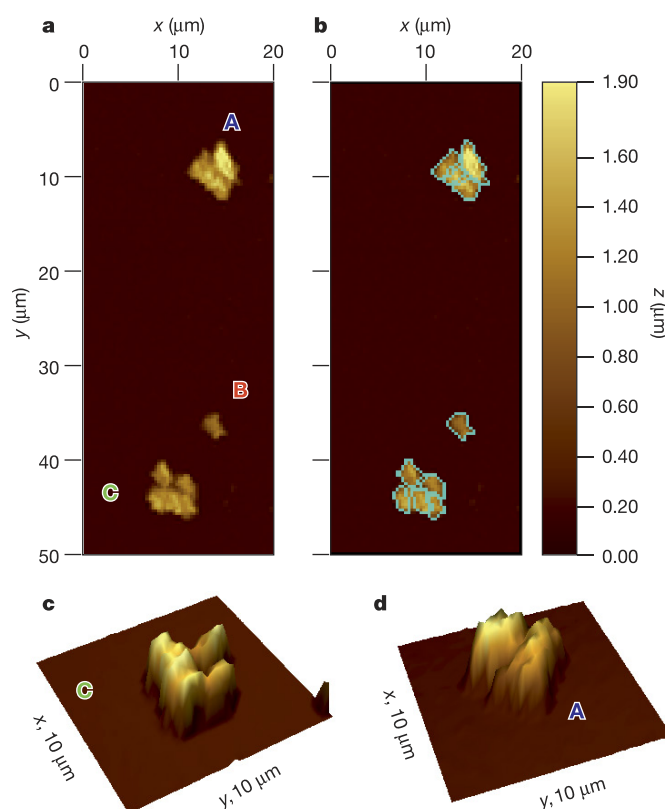

Figure 1 | AFM topographic images of particles A, B and C and their sub-units. a, A 20 μm × 50 μm overview image with a pixel resolution of 312 nm and the colour scale representing the height, *z*. **b**, As in **a**, but with particle B and the sub-units of particles A and C outlined in cyan. **c, d**, 10 μm × 10 μm three-dimensional (rotated) images of particles C and A with two-times height exaggeration to aid visualization.

[1]Space Research Institute, Austrian Academy of Sciences, Schmiedlstrasse 6, 8042 Graz, Austria. [2]Physics Institute, University of Graz, Universitätsplatz 5, 8010 Graz, Austria. [3]European Space Research and Technology Centre, Future Missions Office (SREF), Noordwijk, The Netherlands. [4]UPMC (Sorbonne Université); CNRS/INSU; LATMOS-IPSL, BC 102, 4 place Jussieu, 75005 Paris, France. [5]Institut für Planetologie, Universität Münster, Wilhelm-Klemm-Strasse 10, 48149 Münster, Germany. [6]Leiden Observatory, Postbus 9513, 2300 RA Leiden, The Netherlands. [7]Space Policy Institute, George Washington University, 20052 Washington DC, USA. [8]Department of Lithospheric Research, University of Vienna, Althanstrasse 14, 1090 Vienna, Austria. [9]Natural History Museum, Burgring 7, 1010 Vienna, Austria. [10]Department of Physics and Technology, UiT The Arctic University of Norway, N-9037 Tromsø, Norway.
*These authors contributed equally to this work.

Compact particles A and C are both approximately 5.6 μm in effective diameter (hereafter size; see Methods) and are built from grains in the size range $1.93^{+0.10}_{-1.22}$ μm to $3.31^{+0.06}_{-1.23}$ μm (where the errors are given as the linear addition of the 1σ statistical uncertainty and the systematic uncertainty; see Methods). The compact grain B is $2.76^{+0.07}_{-0.61}$ μm in size, comparable to the dust grains of particles A and C. In fact, the topographic image suggests that grain B was originally part of particle C, but detached on impact with the target. Particle D is $1.09^{+0.01}_{-0.25}$ μm in size, again similar to the grains in A–C. However, the higher resolution reveals that this micrometre-sized particle is itself an aggregate of smaller units; seven grains can be resolved, with sizes ranging from 260^{+50}_{-120} nm to 540^{+20}_{-250} nm. The visible part of particle E has a maximum extent of 14 μm in the x direction and 37 μm in the y direction. Analysis of its component grains (Fig. 3d) shows sizes in the range from $0.58^{+0.15}_{-0.20}$ μm to $2.57^{+0.04}_{-0.51}$ μm, with the grain heights ranging between 0.2 μm and 3 μm and with 90% smaller than 1.7 μm. These measurements are evidence for a continuation of the aggregate nature of dust particles below the size range observed by the COSIMA (Cometary Secondary Ion Mass Analyser) instrument on-board Rosetta (tens to hundreds of micrometres)[15].

Particle E also shows a morphology that is strongly reminiscent of stratospheric, chondritic porous interplanetary dust particles (IDPs), which have long been suspected of having a cometary origin. This link is consistent with observations by COSIMA for larger dust particles, which also measured similar compositions for dust at comet 67P and IDPs[15,16]. One notable difference to IDPs is the extremely flat nature of particle E, which has a height that is an order of magnitude lower than its (minimal) lateral dimension. Indeed, all of the particles presented here have flattened shapes to some degree (see Table 1). It is not yet clear if this is an intrinsic property of cometary dust or the result of a rearrangement of grains on impact. COSIMA has observed that sub-millimetre aggregate particles undergo rearrangement of their grains on impact, producing flattened shapes[15]. Additionally, COSIMA collected small, apparently compact particles that are also flat, but the resolution is insufficient to determine if they are single grains or aggregates. On the other hand, cluster–cluster aggregation with rotating grains can form elongated structures with very high aspect ratios[17], and laboratory experiments have produced dust "flakes"[18].

Investigation of the size distribution of chondritic porous IDPs and fine-grained material returned by the Stardust mission[19,20] showed that the majority of their component grains are smaller than 500 nm (refs 20, 21). Figure 3d shows that 90% of the grains in particle E are smaller than 2 μm, comparable to the size of particle D, which is itself

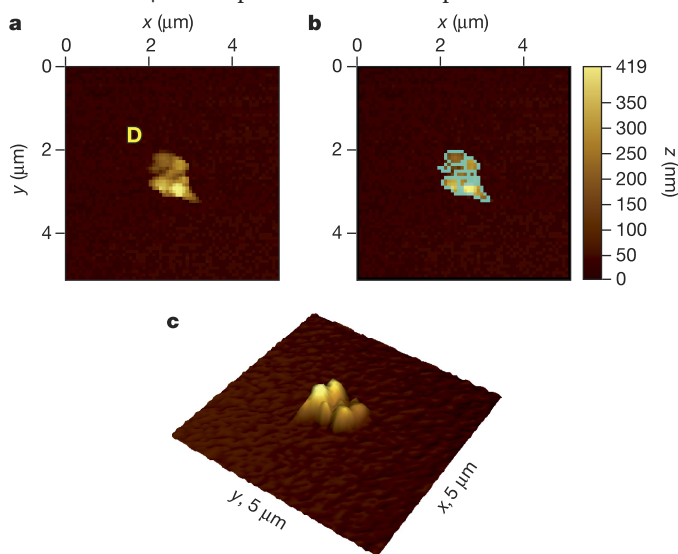built from grains smaller than about 500 nm. This result suggests that the grains of the fluffy aggregate particle E are also aggregates of sub-micrometre components similar to those in chondritic porous IDPs, and points towards a hierarchical structure. Hierarchical growth (that is, aggregates of smaller aggregates) has been proposed as a growth mechanism in the protoplanetary disk when fragmentation of larger particles provides a population of smaller aggregates available for agglomeration[10]. The sticking probability of such particles can be higher than that of homogeneous dust for a given mass and velocity and need to be accounted for in models of dust particle growth[11]. Hierarchical aggregates have also been invoked to produce a surface layer of cometary dust with sufficiently low tensile strength to allow for dust release[12].
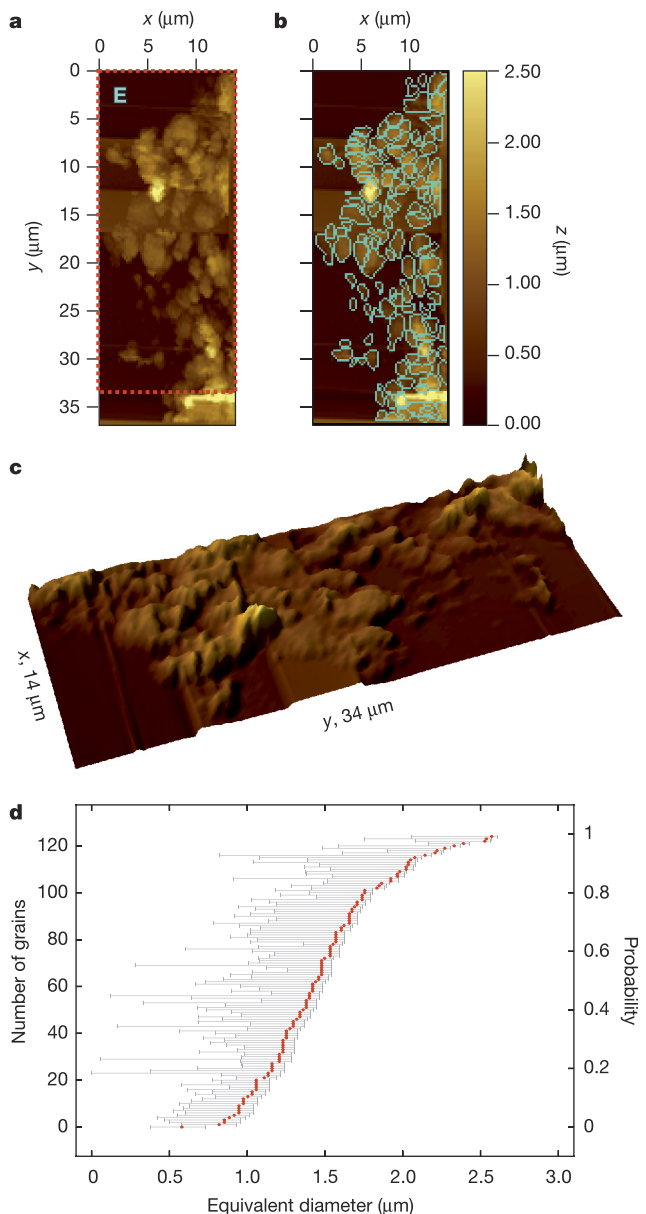

Figure 3 | AFM topographic images of particle E, showing its sub-units and their size distribution. a, A 14 μm × 37 μm overview image with a pixel resolution of 210 nm and the colour scale representing the height, z. **b**, As in **a**, but with identified grains outlined in cyan. **c**, A three-dimensional 14 μm × 34 μm view (corresponding to region indicated by the red dashed box in **a**; rotated and cropped). **d**, Cumulative distribution of the equivalent diameters of the grains (red circles), with error bars in grey (where the errors are given as the linear addition of the 1σ statistical uncertainty and the systematic uncertainty; see Methods). The left scale shows the cumulative number of grains and the right scale shows the probability that particles have equivalent diameters below the specific values.

Figure 2 | AFM topographic images of particle D and its sub-units. a, A 5 μm × 5 μm overview image with a pixel resolution of 80 nm and the colour scale representing the height, z. **b**, As in **a**, but with the sub-units of particle D outlined in cyan. **c**, A three-dimensional (rotated) image of the particle with two-times height exaggeration to aid visualization.

Table 1 | Size, height and elongation of dust particles A–D and their component dust grains

	Type	$d \pm \Delta d$ (µm)	z_{max} (µm)	Elongation
Particle A	Compact particle	$5.48^{+0.04}_{-1.10}$	1.79	$3.32^{+0.14}_{-0.41}$
Grain 1	Dust grain	$3.31^{+0.06}_{-1.23}$	1.79	$2.94^{+0.12}_{-0.43}$
Grain 2	Dust grain	$2.62^{+0.08}_{-0.87}$	1.33	$3.04^{+0.15}_{-0.42}$
Grain 3	Dust grain	$1.93^{+0.10}_{-1.22}$	1.57	
Grain 4	Dust grain	$2.62^{+0.08}_{-1.07}$	1.55	$1.96^{+0.09}_{-0.40}$
Particle B	Dust grain	$2.76^{+0.07}_{-0.61}$	1.02	$3.14^{+0.18}_{-0.42}$
Particle C	Compact particle	$5.79^{+0.04}_{-0.87}$	1.39	$4.77^{+0.24}_{-0.50}$
Grain 1	Dust grain	$2.66^{+0.07}_{-0.92}$	1.33	$2.26^{+0.11}_{-0.42}$
Grain 2	Dust grain	$2.57^{+0.08}_{-0.72}$	1.14	$2.80^{+0.15}_{-0.41}$
Grain 3	Dust grain	$2.18^{+0.09}_{-0.83}$	1.28	$2.23^{+0.12}_{-0.39}$
Grain 4	Dust grain	$2.42^{+0.08}_{-0.90}$	1.39	$2.31^{+0.11}_{-0.39}$
Grain 5	Dust grain	$2.31^{+0.08}_{-0.87}$	1.38	$2.32^{+0.11}_{-0.39}$
Particle D	Compact particle	$1.09^{+0.01}_{-0.25}$	0.42	$3.36^{+0.23}_{-0.47}$
Grain 1	Dust grain	$0.26^{+0.05}_{-0.12}$	0.17	$1.89^{+0.19}_{-0.36}$
Grain 2	Dust grain	$0.48^{+0.03}_{-0.16}$	0.22	$2.52^{+0.20}_{-0.47}$
Grain 3	Dust grain	$0.41^{+0.03}_{-0.14}$	0.31	$1.62^{+0.11}_{-0.27}$
Grain 4	Dust grain	$0.33^{+0.04}_{-0.13}$	0.25	$1.74^{+2.51}_{-0.71}$
Grain 5	Dust grain	$0.46^{+0.03}_{-0.17}$	0.37	$1.53^{+0.09}_{-0.28}$
Grain 6	Dust grain	$0.54^{+0.02}_{-0.25}$	0.42	$2.00^{+5.07}_{-0.82}$
Grain 7	Dust grain	$0.26^{+0.05}_{-0.15}$	0.32	$2.00^{+8.03}_{-0.97}$

d is the diameter of a circle with equivalent area to that of the particle or grain; z_{max} is the maximum height above the substrate surface. The errors of the diameters are given as the linear addition of the 1σ statistical uncertainty and the systematic uncertainty, and the errors of the elongation are given as the worst-case estimate; see Methods for further details. For particle A grain 3 and particle D grains 4, 6 and 7, the maximal elongation is found for the ratio of the two lateral dimensions that are attached with especially large uncertainties. Therefore, an accurate elongation cannot be given for particle A grain 3 and the elongations of the grains of particle D have large uncertainties.

Because MIDAS provides real measurements of the grain shapes, it is possible to evaluate which models support the observations. The elongation of the grains is found by calculating the ratio of the longest and shortest perpendicular axis. Further details are described in Methods. For particle E, the grain heights are almost all smaller than their in-plane diameters, suggesting that it comprises a single layer of grains, allowing accurate grain heights to be determined. The elongation is calculated for 114 grains (the 11 omitted grains show strong distortions due to tip convolution), giving an average elongation of $2.87^{+1.90}_{-0.44}$ (that is, the largest axis is three times longer than the smallest; the uncertainties represent a worst-case estimate containing 1σ statistical errors and systematic uncertainties). The compact particles show similar values (Table 1).

Elongated grains are considered in several models of cometary dust. For example, it has been suggested[22] that comets aggregate from interstellar grains. In ref. 22, the dust grains were modelled as cylinders with aspect ratios of 2–4, and good agreement was found between light scattering experiments and observations. Other works have similarly demonstrated good agreement between simulations using aggregates of spheroidal particles and observational data[23,24]. The elongated nature of interstellar dust can be inferred from linear polarization of starlight due to partially aligned grains[25]. The core–mantle structure proposed for interstellar and cometary dust[26] cannot be confirmed by MIDAS data alone, but the elongation measurement supports the idea of a common precursor grain, or growth mechanism.

Online Content Methods, along with any additional Extended Data display items and Source Data, are available in the online version of the paper; references unique to these sections appear only in the online paper.

1. Dominik, C., Blum, J., Cuzzi, J. & Wurm, G. in *Protostars and Planets V* (eds Reipurth, B. *et al.*) 783–801 (Univ. Arizona Press, 2006).
2. Blum, J. Experiments on sticking, restructuring, and fragmentation of preplanetary dust aggregates. *Icarus* **143**, 138–146 (2000).
3. Dollfus, A. Polarimetry of grains in the coma of 1P/Halley. *Astron. Astrophys.* **219**, 469–478 (1989).
4. Kolokolova, L., Hanner, M. S., Levasseur-Regourd, A. C. & Gustafson, B. A. S. in *Comets II* (eds Festou, M. *et al.*) 577 (Univ. Arizona Press, 2004).
5. Kolokolova, L. & Kimura, H. Comet dust as a mixture of aggregates and solid particles: model consistent with ground-based and space-mission results. *Earth Planets Space* **62**, 17–21 (2010).
6. Hanner, M. S. The scattering properties of cometary dust. *J. Quant. Spectrosc. Radiat. Transf.* **79–80**, 695–705 (2003).
7. Brownlee, D. E. Morphological, chemical and mineralogical studies of cosmic dust [and discussion]. *Phil. Trans. R. Soc. A* **323**, 305–311 (1987).
8. Flynn, G. J. *et al.* Elemental compositions of comet 81P/Wild 2 samples collected by Stardust. *Science* **314**, 1731–1735 (2006).
9. Brownlee, D. *et al.* Comet 81P/Wild 2 under a microscope. *Science* **314**, 1711–1716 (2006).
10. Dominik, C. Physical processes : dust coagulation and fragmentation. in *ASP Conf. Ser.* Vol. 414 (eds Henning, T. *et al.*) 494–508 (Astronomical Society of the Pacific, 2009).
11. Johansen, A. *et al.* in *Protostars and Planets VI* (eds Beuther, H. *et al.*) 547–570 (Univ. Arizona Press, 2014).
12. Skorov, Y. & Blum, J. Dust release and tensile strength of the non-volatile layer of cometary nuclei. *Icarus* **221**, 1–11 (2012).
13. Bentley, M. S. *et al.* MIDAS : lessons learned from the first spaceborne atomic force microscope. *Acta Astronaut.* **125**, 11–21 (2016).
14. Riedler, W. *et al.* MIDAS — the micro-imaging dust analysis system for the Rosetta mission. *Space Sci. Rev.* **128**, 869–904 (2007).
15. Langevin, Y. *et al.* Typology of dust particles collected by the COSIMA mass spectrometer in the inner coma of 67P/Churyumov Gerasimenko. *Icarus* **271**, 76–97 (2016).
16. Hilchenbach, M. *et al.* Comet 67P/Churyumov–Gerasimenko: close-up on dust particle fragments. *Astrophys. J.* **816**, L32 (2016).
17. Paszun, D. & Dominik, C. The influence of grain rotation on the structure of dust aggregates. *Icarus* **182**, 274–280 (2006).
18. Stephens, J. R. & Gustafson, B. Å. S. Laboratory reflectance measurements of analogues to "dirty" ice surfaces on atmosphereless solar system bodies. *Icarus* **94**, 209–217 (1991).
19. Rotundi, A. *et al.* Combined micro-Raman, micro-infrared, and field emission scanning electron microscope analyses of comet 81P/Wild 2 particles collected by Stardust. *Meteorit. Planet. Sci.* **43**, 367–397 (2008).
20. Stodolna, J., Gainsforth, Z., Butterworth, A. L. & Westphal, A. J. Characterization of preserved primitive fine-grained material from the Jupiter family comet 81P/Wild 2 — a new link between comets and CP-IDPs. *Earth Planet. Sci. Lett.* **388**, 367–373 (2014).
21. Wozniakiewicz, P. J., Bradley, J. P., Ishii, H. A., Price, M. C. & Brownlee, D. E. Pre-accretional sorting of grains in the outer solar nebula. *Astrophys. J.* **779**, 164 (2013).
22. Greenberg, J. M. & Gustafson, B. Å. S. A comet fragment model for zodiacal light particles. *Astron. Astrophys.* **93**, 35–42 (1981).
23. Levasseur-Regourd, A. C., Mukai, T., Lasue, J. & Okada, Y. Physical properties of cometary and interplanetary dust. *Planet. Space Sci.* **55**, 1010–1020 (2007).
24. Lasue, J. & Levasseur-Regourd, A. C. Porous irregular aggregates of sub-micron sized grains to reproduce cometary dust light scattering observations. *J. Quant. Spectrosc. Radiat. Transf.* **100**, 220–236 (2006).
25. Mathis, J. S. Interstellar dust and extinction. *Annu. Rev. Astron. Astrophys.* **28**, 37–70 (1990).
26. Greenberg, J. M. & Hage, J. I. From interstellar dust to comets: a unification of observational constraints. *Astrophys. J.* **361**, 260–274 (1990).

Author Contributions R.S., T.M. and M.S.B. planned the experiments on MIDAS, analysed and interpreted the data and wrote the manuscript. M.S.B. developed the planning and data processing pipelines. R.S. and T.M. implemented the elongation calculations. R.S. performed the post-processing and calibration as well as the particle/grain measurement and is responsible for the graphical data presentation. T.M. considered the uncertainties for all data. A.-C.L.-R. provided information on cometary dust derived from polarimetric observations and its interpretation. H.J. supported the experiments with software updates. All authors discussed the results and commented on the manuscript.

METHODS

Data acquisition and calibration. Exposure durations and times were planned by estimating the dust flux using the predicted spacecraft position, pointing and a dust flux model for comet 67P derived from observational data[27]. For a graphical visualization of the exposure geometries, see Extended Data Figs 1–3.

MIDAS operates in a slightly different way from most terrestrial AFMs, by making a careful approach to the sample at each pixel position and then moving away by a so-called retraction distance before moving to the next pixel, resulting in long scan times and possible distortion[13,14]. Distortion correction is performed using scans of on-board calibration targets, and polynomial background correction is used to remove height drifts. This procedure was performed with the data used to produce Figs 1 and 3. The scan shown in Fig. 2 was much shorter and no substantial distortion was observed; hence, only background subtraction was performed. Particle and grain heights are measured relative to the substrate surface, which is very clear for Figs 1 and 2, but the zero reference level had to be set manually for each grain in Fig. 3, because the steps would otherwise distort the measurements.

The lateral extent of particles and grains is characterized by an effective size (d), which is the diameter of a circle with the same area as the projection of all pixels forming the unit; unless stated otherwise, all references to size refer to this effective value. The peak height (z_{max}) is the maximum elevation above the target for a given grain. Identification of particles and their sub-units is performed by visual inspection of the calibrated data and, when necessary, cross-sections through the three-dimensional data are used; see Extended Data Fig. 4.

For particle E (Fig. 3), a manual levelling of the surface was necessary, owing to the visible steps (imaging artefacts). Repeating this manual levelling process several times showed that the induced error was negligible. In addition, the height of a grain can be measured precisely only if the grain is directly on the surface and not on another grain. For particle E, most of the grains seem to fulfil this requirement, because the mean heights of the grains are smaller than their mean diameters.

**Error analysis.** In principle, because AFM tips cannot be infinitely sharp, the size of every particle is overestimated, owing to the tip sample convolution (that is, the recorded image reflects a combination of tip and sample shapes). For example, a cone-shaped tip with a large opening angle artificially broadens features, as depicted in Extended Data Fig. 5. The convolution uncertainty is generously estimated here to give an upper limit. Because the particle diameter cannot be underestimated by this convolution, the uncertainty interval becomes asymmetric. This systematic uncertainty is linearly added to the 1σ statistical uncertainty generated by the identification of the grains in the scan. Values for sizes and respective uncertainties quoted in the text for all particles, depicted in Fig. 3d for particle E and presented in Table 1 for particles A–D, reflect this calculation.

The elongation of particles and grains is calculated by determining their equivalent ellipse (the ellipse with the same second-order moments) and choosing the maximum ratio of the largest to smallest of (i) the height of the particle to the major axis, (ii) the height to the minor axis and (iii) the ratio of the major and minor axes. The uncertainties in these ratios take into account the 1σ statistical uncertainty due to the manual masking of the particles and the systematic uncertainty due to the tip–sample convolution for the axis lengths. The ratio of the major to minor axis suffers from a large convolution uncertainty that, in some cases (typically particles with steep slopes), prevents a clear statement about the orientation. In these cases, no elongation is given. The final uncertainty for the ratio is a worst-case estimate that overestimates the uncertainty for non-isolated flat grains.

Code and data availability. Extended Data Table 1 summarizes the key parameters for the AFM scans used to produce Figs 1–3. The filenames listed refer to products available in the ESA Planetary Science Archive where all data used here are freely available (http://www.cosmos.esa.int/web/psa/rosetta). The open-source package Gwyddion[28] was used to perform calibration, grain identification and analysis throughout this paper (http://gwyddion.net/).

27. Fulle, M. *et al.* Comet 67P/Churyumov–Gerasimenko: the GIADA dust environment model of the Rosetta mission target. *Astron. Astrophys.* **522,** A63 (2010).
28. Nečas, D. & Klapetek, P. Gwyddion: an open-source software for SPM data analysis.*Cent. Eur. J. Phys.* **10,** 181–188 (2012).
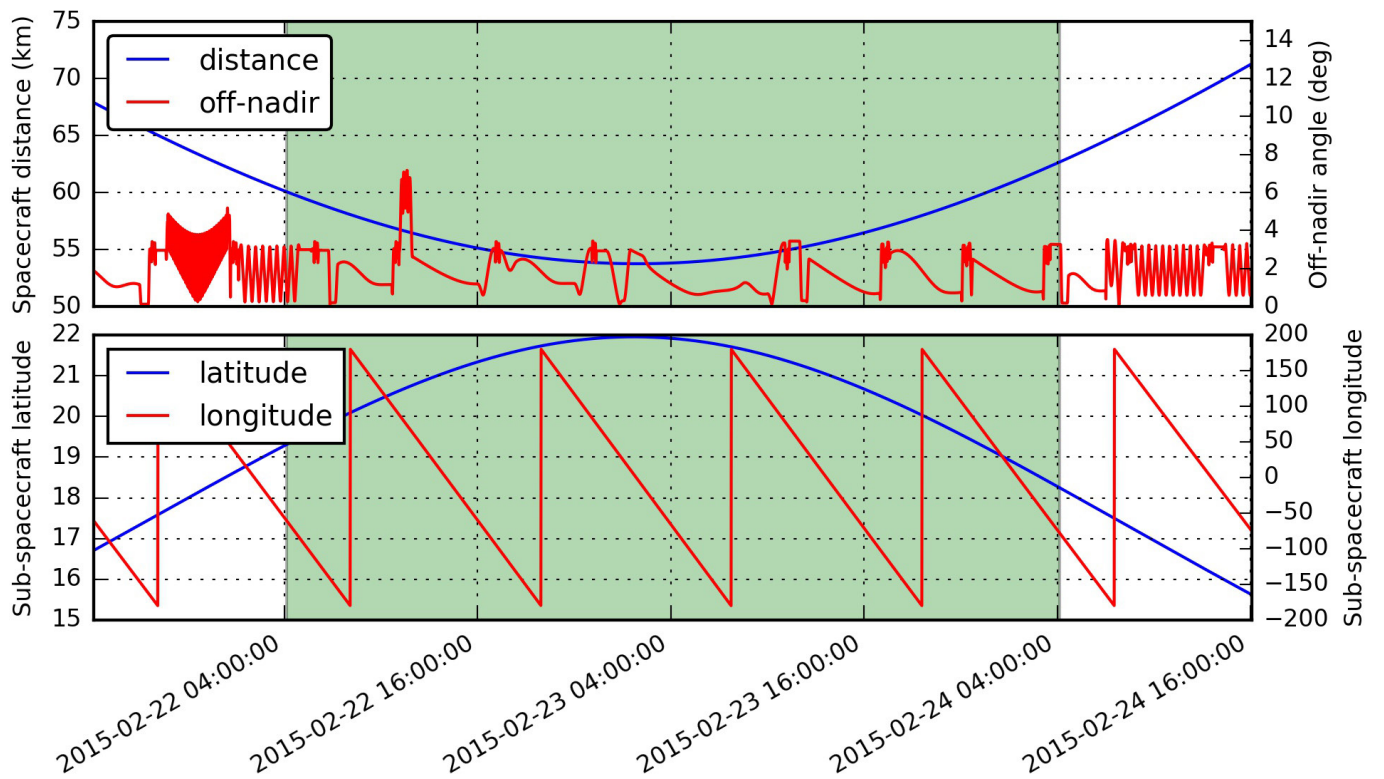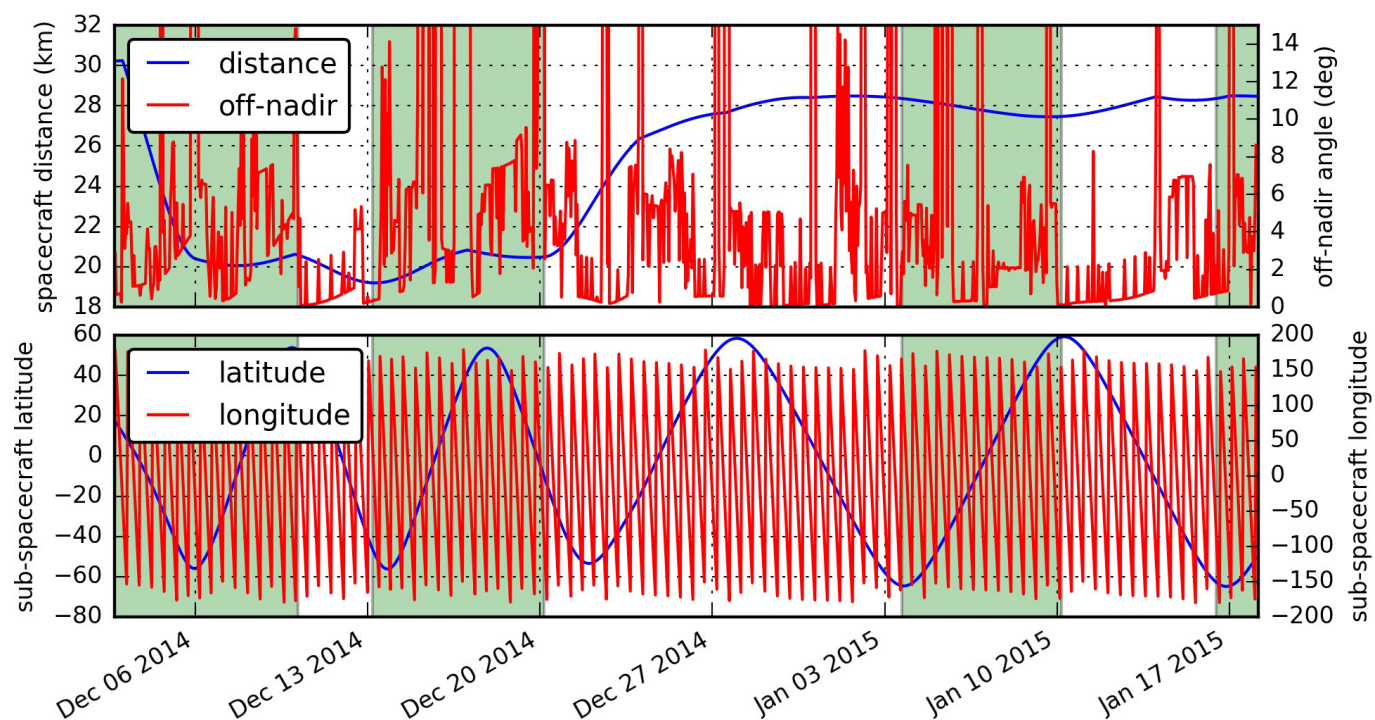
Extended Data Figure 1 | The geometry of the exposures where particles A, B and C were collected. All exposures are marked by green bars. The top panel shows the distance of Rosetta from the comet (blue) and the off-nadir angle (red). The lower panel shows the latitude and longitude of the point on the comet below the spacecraft (the sub-spacecraft latitude and longitude) in blue and red, respectively. The heliocentric distance (between the comet and the Sun) during this exposure was 2.25 au.
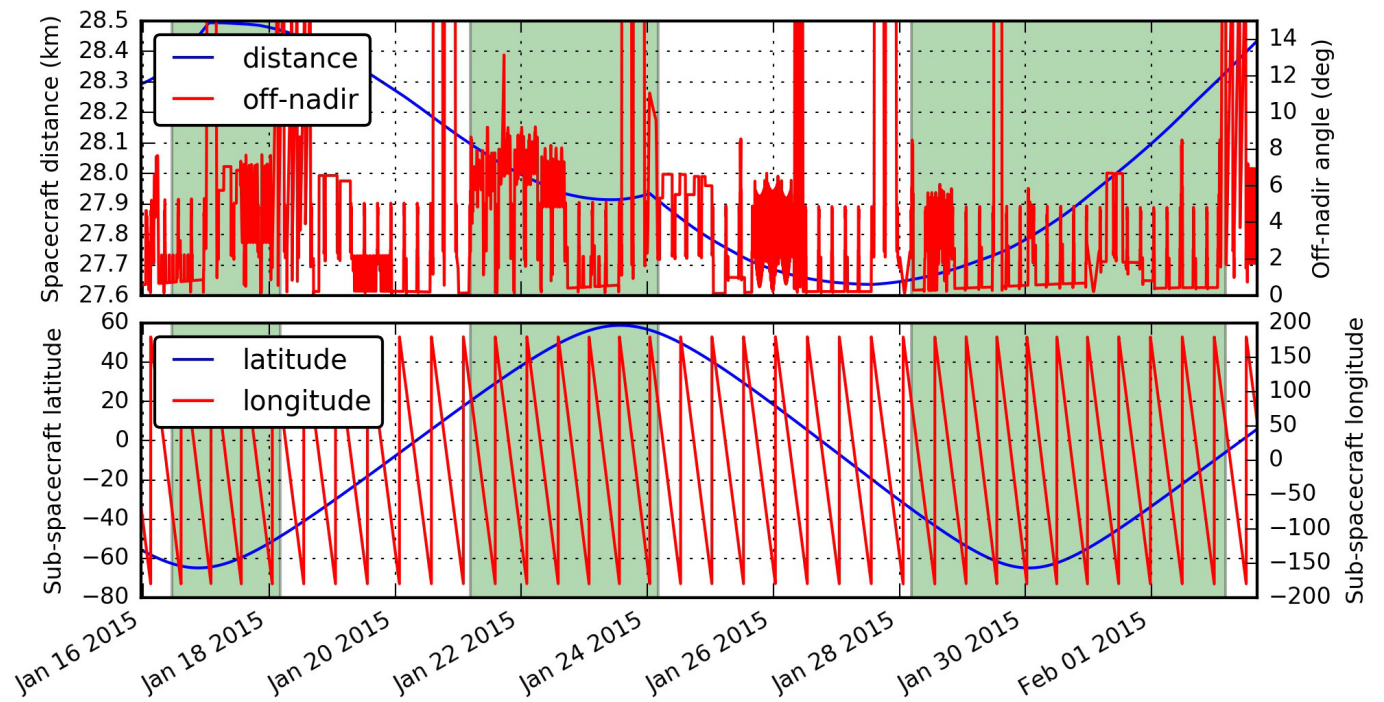
Extended Data Figure 2 | The geometry of the exposures where particle D was collected. All exposures are marked by green bars. The top panel shows the distance of Rosetta from the comet (blue) and the off-nadir angle (red). The lower panel shows the sub-spacecraft latitude and longitude in blue and red, respectively. The heliocentric distance during this exposure varied between 2.54 au and 2.41 au.
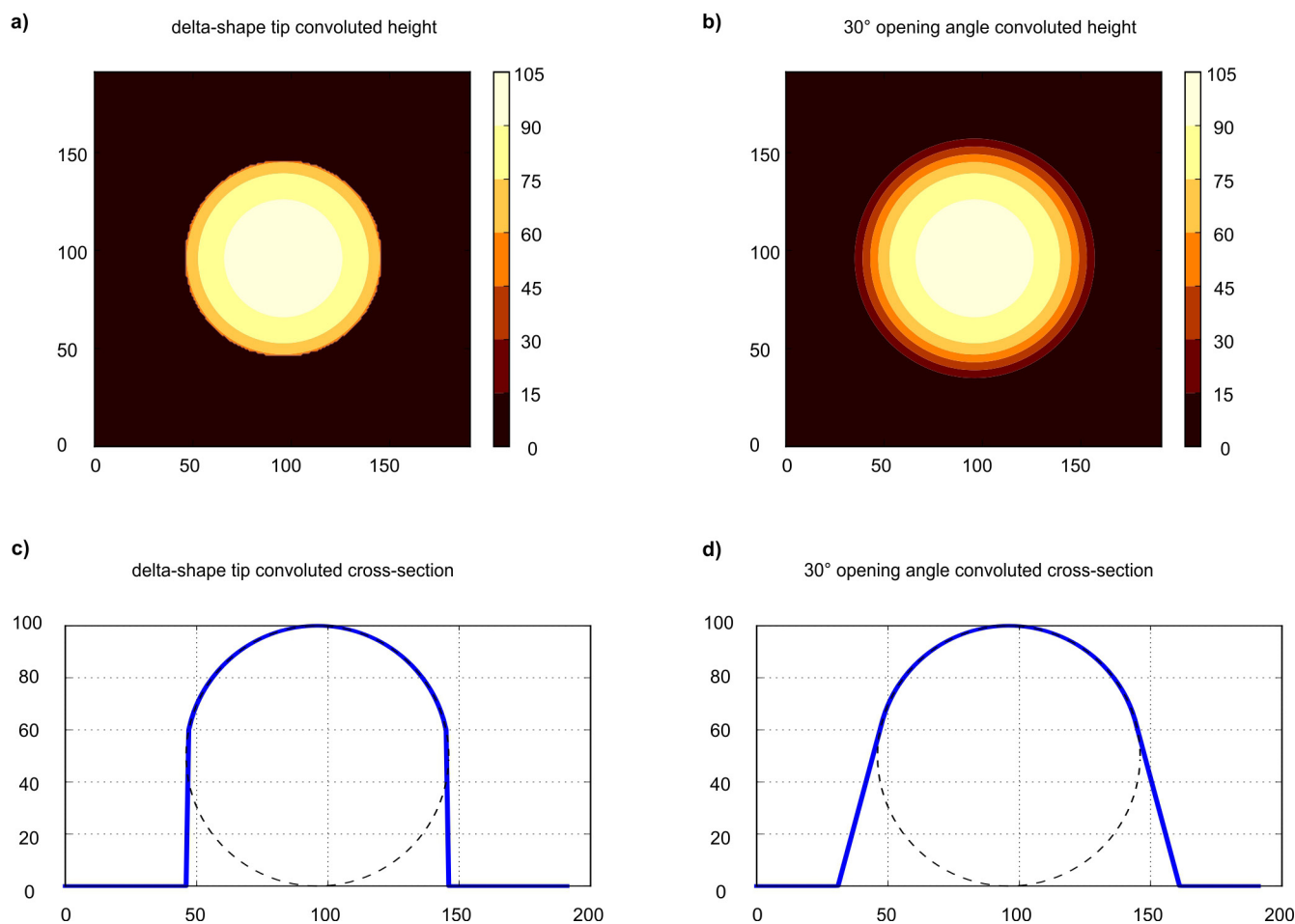
Extended Data Figure 3 | The geometry of the exposures where particle E was collected. All exposures are marked by green bars. The top panel shows the distance of Rosetta from the comet (blue) and the off-nadir angle (red). The lower panel shows the sub-spacecraft latitude and longitude in blue and red, respectively. The heliocentric distance during this exposure varied between 2.85 au and 2.52 au.

a)

b)
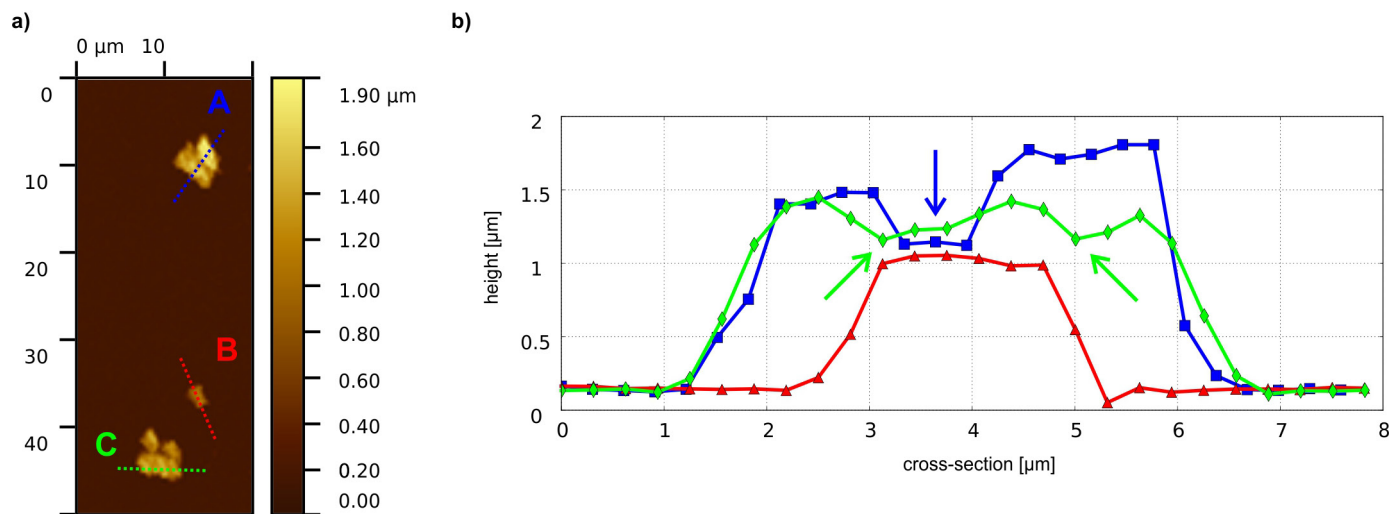
Extended Data Figure 4 | Topographic cross-sections demonstrating the identification of sub-units. a, Topographic image of particles A, B and C. Dashed blue, red and green lines show where the cross-sections of particle A, B and C, respectively, were made. The colour scale represents the height. **b**, Height profiles of the three cross-sections shown in **a**, demonstrating how sub-grains were identified (blue and green arrows) and revealing slopes of 60°–70° with the substrate surface.

a) delta-shape tip convoluted height

b) 30° opening angle convoluted height

c) delta-shape tip convoluted cross-section

d) 30° opening angle convoluted cross-section

Extended Data Figure 5 | Tip–sample convolution effects.
a, b, Simulated AFM images (colour scale indicates the height) providing a comparison between a spherical particle imaged with an ideal, infinitely sharp tip (**a**) and with a cone-shaped tip with an opening angle of 30° (**b**), which is similar to that of the MIDAS tips[14]. **c, d,** The corresponding cross-sections through the centre of the structures (*y* axis shows the height). The black dashed curves show the spherical particle and the blue lines depict the topography as measured with infinitely sharp and cone-shaped tips, respectively. The measurement of the volume of the spherical particle is exaggerated by 25% for the delta-shaped tip and by 50% for the cone-shaped tip. The maximum height measurement is not affected by the tip–sample convolution.

Extended Data Table 1 | Scan parameters of the primary AFM topography scans shown in Figs 1–3

	Figure 1	Figure 2	Figure 3
target	14	12	12
cantilever	9	9	7
image resolution	256 x 256	256 x 256	192 x 192
image size	80 x 80 µm²	20 x 20 µm²	40 x 40 µm²
pixel resolution	312 nm	80 nm	210 nm
z step size	0.7 nm	0.7 nm	0.7 nm
retraction height	1095 nm	977 nm	734 nm
duration	1 day, 05:05:33	08:14:15	11:16:30
start time	2015-04-29T05:21:40Z	2015-03-13T08:44:38Z	2015-01-18T20:59:28Z
filename	IMG_1509813_1512600_054_ZS	IMG_1507001_1508813_005_ZS	IMG_1501323_1504200_013_ZS

The number of pixels and the pixel resolution at a given scan size was limited by the time available and chosen to maximize the resolution. The filename corresponds to that used in the Planetary Science Archive.